Crystal structure and enhanced magneto-electric properties of cobalt-substituted nickel–zinc ferrite

Xiao-Hui Wu[1], Zheng-Xiong Tao[1], Le-Zhong Li[1,*] ⬤, Chong-Sheng Wu[2], Xiao-Xi Zhong[1], Rui Wang[1], Peng-Cheng Xiang[1], Ke-Lin Li[1], and Nan Lin[1]

[1] *Sichuan Province Key Laboratory of Information Materials and Devices Application, College of Optoelectronic Engineering, Chengdu University of Information Technology, Chengdu 610225, People's Republic of China*

[2] *Department of Electrical and Computer Engineering, Center for Microwave Magnetic Materials and Integrated Circuits (CM3IC), Northeastern University, Boston, MA 02115, USA*

ABSTRACT

In this work, $Ni_{0.7-x}Zn_{0.3}Co_xFe_2O_4$ (x = 0, 0.05, 0.10, 0.15 and 0.20, NZCF) ferrites were successfully fabricated by solid-state reaction method. We have been more focused on the effects of cobalt-substituted NiZn ferrite on crystal structure, microstructure and magneto-electric properties. With gradual addition of cobalt content, since the smaller ionic radius and larger atomic weight of the cobalt, which leads to decrease lattice parameter (a) and enhance X-ray density (d_x), respectively. The grain size (D) increases (4.86 ± 1.10 to 6.26 ± 1.67 μm). When x = 0.05, the initial permeability (μ_i) of NiZnCo ferrites reaches the maximum value. The saturation magnetization (Ms) is firstly decreased slightly from 78.96 to 77.96 emu/g when $x \leq 0.10$, then increased to 83.14 emu/g (x = 0.15), ultimately decreased to 81.54 emu/g. Meanwhile, the coercivity (Hc) is dropped from 19.95 to 13.25 Oe when $x \leq 0.05$, and stabilized at about 13.40 Oe when $x > 0.05$. From the dielectric spectrum, the real dielectric constant (ε') exhibits typical relaxation-dispersion behavior with increasing frequency. The resistivity temperature spectrum also shows good performance: both dc resistivity (ρ) and activation energy (E_ρ) increase with the Co substitution. Here, we have developed a NiZnCo ferrite when Co-substituted x = 0.05 with the highest permeability (μ_i, 123@10 kHz), higher saturation magnetization (Ms, 78.25 emu/g) and lowest coercivity (Hc, 13.25Oe), which is expected to be used in high-frequency capacitors and inductors.

Address correspondence to E-mail: lezhongli@cuit.edu.cn

⚛ Springer

1 Introduction

Based on the development needs of new electronic information materials, ferrimagnetic materials have attracted the attention of many scientific researchers due to their excellent electromagnetic performance: high initial permeability, high saturation magnetization, low coercivity, low dielectric loss, high electrical resistivity and good chemical properties. Therefore, these can be expected to be applied to inductors, transformers, magnetic coils, and magnetic recording devices [1–4].

However, electromagnetic properties are susceptible to many factors for chemical composition, preparation method, metal cation substitution and various dopants. One of the simplest and most efficient ways to enhance electromagnetic performance is through substituting the metal cation on the tetrahedron (A site) or octahedron (B site) [5–7]. As is known to all, NiZn ferrite stands out among many ferrimagnetic materials applying electronic equipment due to its high initial permeability, high saturation magnetization, low coercivity and high resistivity. The inductors and transformers have been implemented from NiZn ferrite [8]. NiZn ferrite has a mixed spinel structure, which is actually composed of 8 A sites and 16 B sites metal-cationic unit cells. Ni^{2+} ions and Fe^{3+} ions take up in B site [9], and Zn^{2+} ions in A site [10]. Since Co^{2+} ions are preferred to occupy position B, change the metal cation distribution inside NiZn ferrite to improve the electromagnetic performance, which can be used in microwave and magnetic head devices [11]. Li et al. studied Co substitution enhances saturation magnetization (Ms) and coercivity (Hc) for NiCu ferrite [12]. It is well explained that the variation of Ms is caused by the difference of magnetic moment due to the difference of ion occupancy distribution [13]. Since the Co^{2+} ions have positive magneto-crystalline anisotropy (K_1), it is possible to appropriately increase the Ms and reduce the Hc, which is well reflected in the research report of Rajinder Kumar et al. [14].

In this work, Co-substituted NiZn ferrite were successfully fabricated by solid-state reaction method. We have been systematically studied with the structural, magnetic and electrical properties for different Co^{2+} substitution after sintering 1300 °C. It was found that when $x = 0.05$, NiZn ferrite has high initial magnetic permeability, moderate saturation magnetization, low coercive force and relatively high direct-current resistivity, which are expected to be applied to electronic components such as inductors, transformers and filters.

2 Experimental procedure

$Ni_{0.7-x}Zn_{0.3}Co_xFe_2O_4$ ($x = 0$, 0.05, 0.10, 0.15 and 0.20, NZCF) ferrites were prepared by solid-state reaction method. The experimental materials were high purity NiO, ZnO, Fe_2O_3 and Co_3O_4 from Aladdin Reagent (Shanghai) Co., Ltd., and the purity was higher than 99.9%. According to the stoichiometric formula, the mass of each raw material was calculated. The weighed materials were mixed for 6 h with the stainless-steel balls. The wet powder was dried in an oven at 80 °C and then pre-burned at 1050 °C for 2 h. Then the calcined powder needs a secondary ball-milling for 8 h. These powders were pressed into toroids (Φ12 mm × Φ8 mm × h5 mm) at 16 MPa and disks (Φ10 mm × h5 mm) at 8 MPa by 8 wt% poly-vinyl alcohol (PVA), respectively. Finally, these toroids and disks were sintered at 1300 °C for 4 h in air. The sintered toroids were tested for initial permeability (μ_i) and the cross-sectional microstructure of SEM images. The sintered disks were measured for dielectric constant (ε') and direct-current resistivity ρ, also were polished into small sphere (Φ4 mm) to test the hysteresis loop.

The crystal phase and images of cross-sectional structure were obtain by XRD (DX 2700, Cu target) and SEM (JEOL JSM-6490L), respectively. The saturation magnetization and coercivity were tested by VSM (Lake Shore 8604) using a magnetic field of 5000 Oe. The LCR Meter Bridge (WK 6500P) was adopted for measuring initial permeability at 10 kHz and dielectric constant. The dc resistivity was measured by high resistance meter (Keithley 6517B) from 50 to 230 °C. Crystal structure parameters, microstructure, magnetic parameters and dielectric parameters were all measured at room temperature, only resistivity parameter was measured at variable temperature.

3 Results and discussion

3.1 Crystal structure characteristics

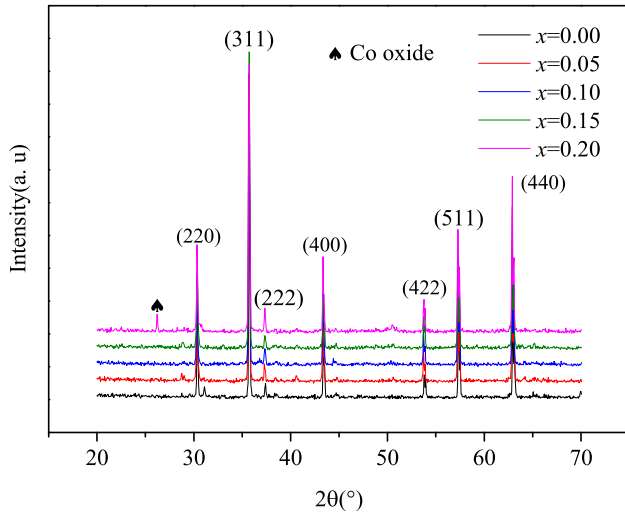Figure 1 displays the XRD patterns of NZCF ($x = 0$, 0.05, 0.10 and 0.15) ferrites which proves that all

Fig. 1 XRD crystal phase spectrum of NZCF ferrites

samples are cubic spinel structure, and the characteristic peaks well match with the previous work [15]. These characteristic peaks are well matched with standard NiZn ferrite cards (JCPDS cards: #52-0278). All samples for NZCF ferrite are exhibited the single spinel phase except when Co substitution $x = 0.20$. However, the impurity phase (Co oxide) appears when $x = 0.2$, because the excessive Co addition and sintering temperature is greater than 1200 °C, easy to form an impurity phase of hexagonal phase, this structure is no longer a single spinel phase. The values of lattice parameter (a) and X-ray density (d_x) are listed in Table 1. a reduces from 0.8369 to 0.8354 nm, d_x rises from 5.408 to 5.417 g/cm^3. The contraction of the lattice is mainly due to the fact that Co^{2+} ion radius (0.065 nm) is smaller than Ni^{2+} ion radius (0.069 nm). This also fully illustrates that Co^{2+} ion enters the octahedral sub-lattice of NiZn ferrite, because it prefers the B site. The high atomic mass of Co^{2+} ions (58.933) replaces the low atomic mass of

Table 1 Crystallographic (lattice parameter a, X-ray density d_x) and Physical parameters (bulk density d, porosity P) of NZCF ferrites

x	a (nm)	d (g/cm^3)	d_x (g/cm^3)	P (%)
0.00	0.8369	5.105	5.408	5.603
0.05	0.8357	5.218	5.410	3.549
0.10	0.8356	5.172	5.413	4.452
0.15	0.8354	5.183	5.416	4.302
0.20	0.8354	5.196	5.417	4.079

Ni^{2+} ions (58.693), which makes the d_x increase slightly with the of Co substitution.

3.2 Microstructure characteristics

The images of cross-sectional structure of NZCF ferrites are reflected in Fig. 2a–e. Since the grain growth promoted by the increase of CoO (Co$_3$O$_4$ will be decomposed into CoO over 1200 °C), Fig. 2f also well illustrates the overall increase in average grain size (D) from 4.86 ± 1.10 to 6.26 ± 1.67 μm. For the NZCF ferrites with $x = 0.15$ Co substitution, the grains perform good uniformity and the largest size of 6.62 ± 2.05 μm. It is important to emphasize that large particles are surrounded by small particles, especially the cobalt substitution content is less than 0.15 for NZCF ferrites, which is typical large grains growth at the expense of small ones [16]. In addition, considering the porosity (P) of pure and Co-substituted NiZn ferrites from Table 1, which indicates that the microstructure of Co-substituted NiZn ferrites is more densified.

3.3 Magnetic properties

Figure 3 shows the variation in initial permeability (μ_i) of NZCF ferrites with different Co substitution contents. μ_i achieves the maximum value (123@10 kHz) at $x = 0.05$. Due to the largest density (d) and the smallest porosity (P) when $x = 0.05$ (see Table 1), the magnetic domain transfer becomes easier, so that the appropriate cobalt substitutions are able to increase the μ_i of NiZn ferrite. Moreover, Co^{2+} ions have positive magneto-crystalline anisotropy constant (K_1), while the K_1 of NiZn ferrite is negative. With appropriate amount of Co substitution, the K_1 of Co-based NiZn ferrite is close to zero, which is another reason for the increase of μ_i. Meanwhile, due to excessive cobalt substitution ($x \geq 0.05$), the magnetic domains inside NiZn ferrite are frozen [17], and it is difficult for the domain wall movement and domain rotation, so that the μ_i drops sharply.

Figure 4a–e exhibit the Hysteresis loop diagram corresponding to different cobalt substitutions for NZCF ferrites. Simultaneously, the values of saturation magnetization (Ms) and coercivity (Hc) with different cobalt substitutions (x) obtained from M-H loops are displayed in Fig. 4f. The Ms is firstly decreased slightly from 78.96 to 77.96 emu/g when $x \leq 0.10$, then increased to 83.14 emu/g ($x = 0.15$),

Fig. 2 SEM images **a** $x = 0$, **b** $x = 0.05$, **c** $x = 0.10$, **d** $x = 0.15$, **e** $x = 0.20$, average grain size and standard deviations (**f**) of NZCF ferrites
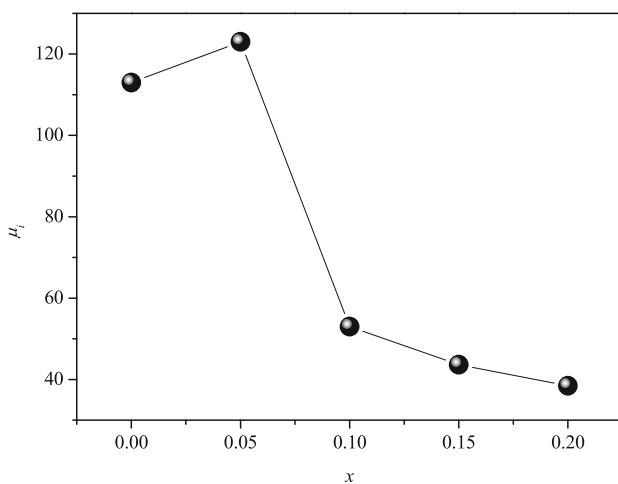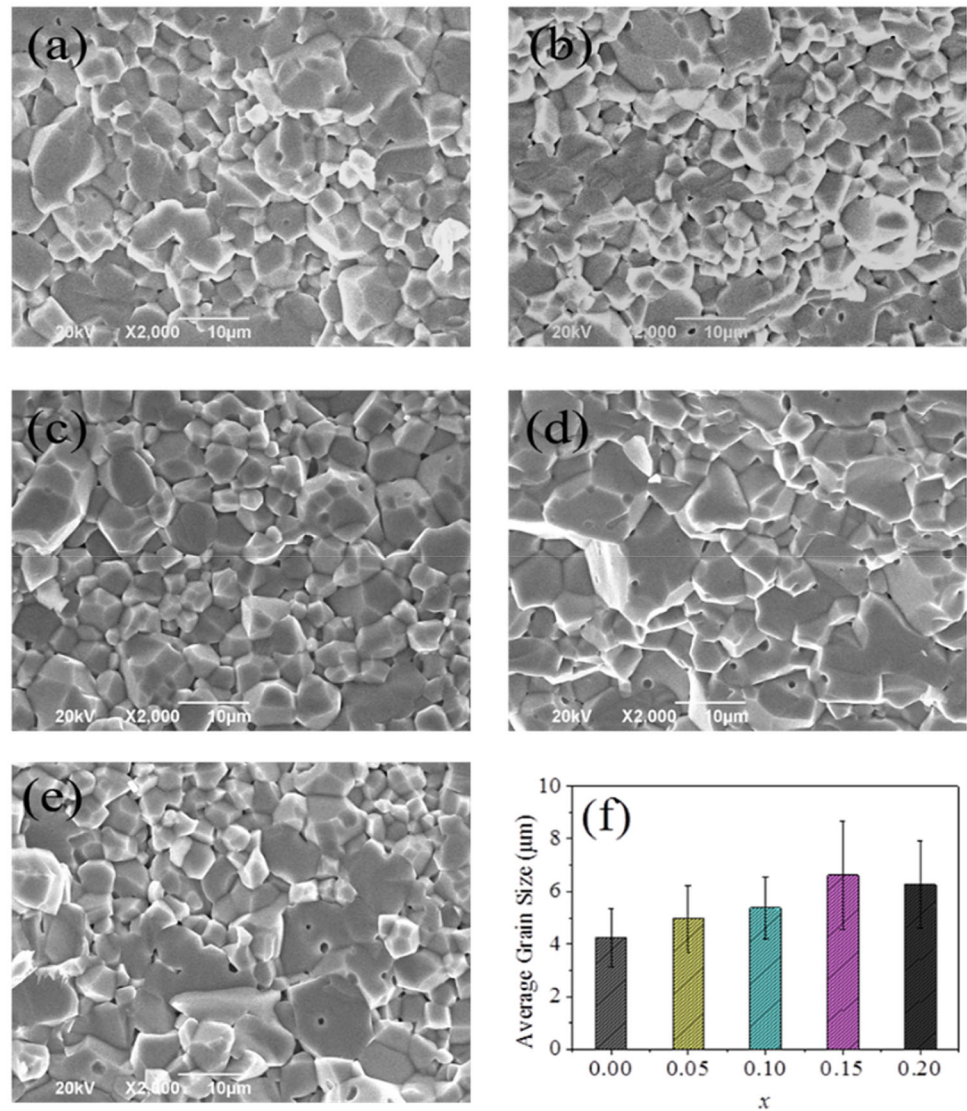

Fig. 3 μ_i with different Co substitution of NZCF ferrites

ultimately decreased to 81.54 emu/g ($x = 0.20$). Also, the Hc drops from 19.95 to 13.25 Oe when $x \leq 0.05$, and stabilized at about 13.40 Oe when $x > 0.05$. However, in general, the Ms increases when $x \leq 0.15$ due to the growth of crystal grains, which is well agreed with the change in the SEM image as seen in Fig. 2f [18]. Then, the decrease of Ms can be attributed that magnetic properties decrease with grain reduction when $x = 0.20$. Coercivity (Hc) is easily limited by grain size, and Hc is proportional to $1/D$ [19]. So, due to D increases from 4.86 ± 1.10 to 6.26 ± 1.67 μm, which leads to a decrease in Hc.

Meanwhile, the related application literature and compiled some related applications for comparison, as shown in Table 2 below. It can be seen from Table 2 that the magnetic parameters can be adjusted

Fig. 4 Hysteresis loop diagram of NZCF ferrites **a** $x = 0$, **b** $x = 0.05$, **c** $x = 0.10$, **d** $x = 0.15$, **e** $x = 0.20$. Values of (Ms) and coercivity (Hc) of NZCF ferrites (**f**) corresponding to different cobalt substitutions
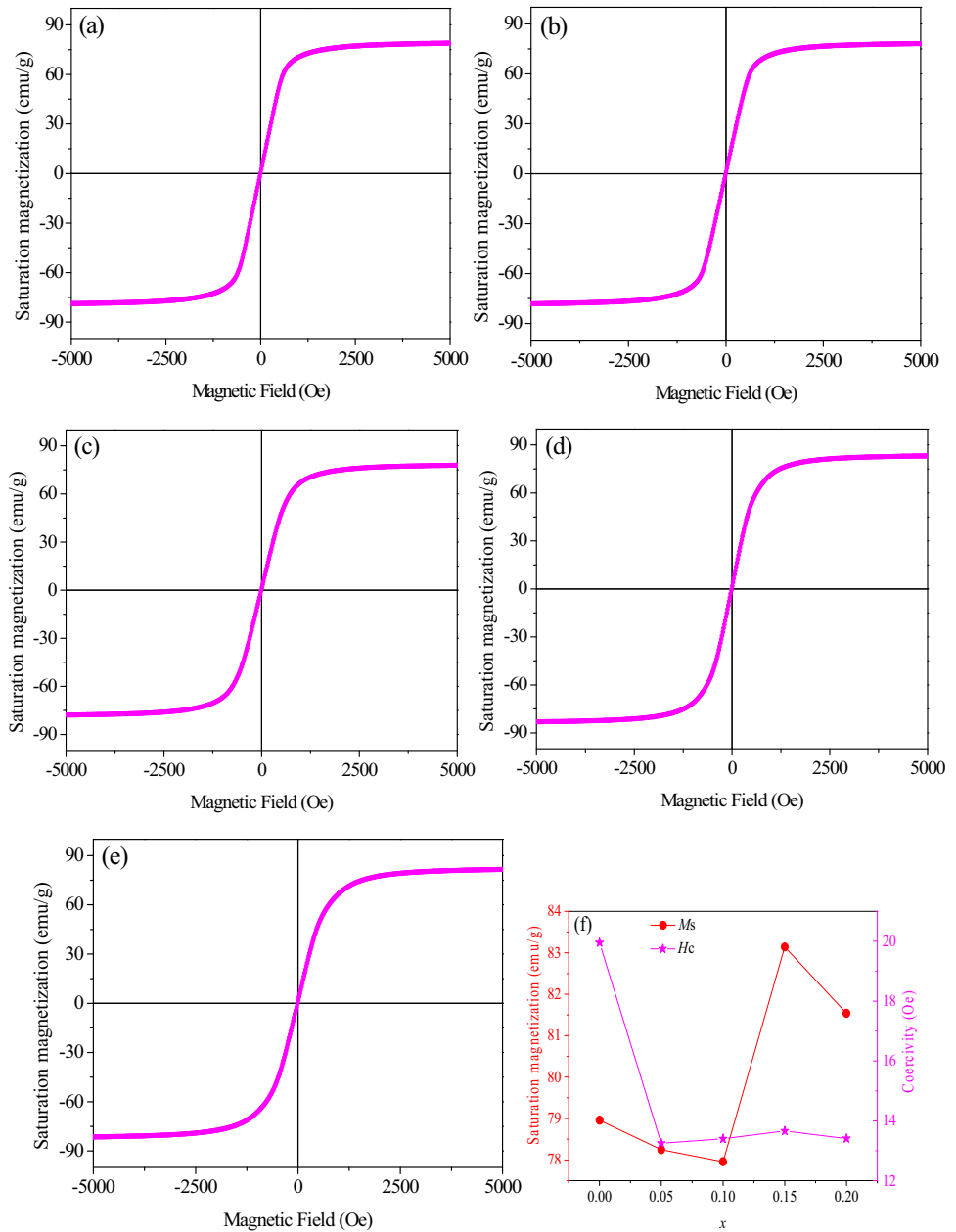

Table 2 Comparison of some ferrite magnetic parameters (saturation magnetization:Ms and coercivity: Hc) for device applications

Ferrite composition	Ms (emu/g)	Hc (Oe)	Refs.
$Ni_{0.5}Zn_{0.5}Fe_2O_4$	72.07	1.85	[20]
$Ni_{0.5}Zn_{0.5}Sm_{0.01}Fe_{1.9}O_4$	55.51	3.72	[20]
$Ni_{0.5}Zn_{0.5}Zr_{0.4}Cu_{0.4}Fe_{1.2}O_4$	32.71	78.12	[21]
$Ni_{0.7}Zn_{0.3}Cr_{0.5}Ce_{0.02}Fe_{1.48}O_4$	12.51	198.37	[22]
$Mn_{0.5}Zn_{0.5}Nd_{0.1}Fe_{1.9}O_4$	23.65	–	[23]
$CoNb_{0.1}Fe_{1.9}O_4$	45.78	548	[24]
$Ni_{0.55}Zn_{0.3}Co_{0.15}Fe_2O_4$	83.14	13.66	This work

by substituting different ions for ferrites. By comparing ferrites with different composition, this work has replaced NiZn ferrites with Co^{2+} ions showing higher saturation strength Ms and lower coercivity

H_c, these magnetic parameters are better than previous studies, so these results can be used for high-frequency inductors/capacitors.

The real dielectric constant (ε') depend on frequency are presented in Fig. 5. It has been clearly seen ε' has larger value (100 Hz) and lower value (more than 100 kHz). The Koop's theory and Maxwell model indicate that charge migration between Fe^{2+} and Fe^{3+} ions leads to polarization, and the dielectric material consists of conductive grains separated by thin resistive grains, which causes the charge to be deposited under the induction of an electric field, forming a space charge polarization [25–27]. Some low-energy electrons can be locally displaced under the action of the external field, thus the polarization contributes to ε', and the more low-energy electrons at low frequencies, the higher the ε'. Moreover, when the frequency increases (in the high frequency band), the electrons participating in polarization will not have time to shift, and the polarization will be weakened, so ε' drops sharply to a stable minimum value. In particular, as the addition of cobalt substitution, ε' gradually decreases, which may be because the third ionization energy of Co (33.77 eV) is lower than Ni (35.92 eV) but higher than Fe (31.69 eV). Therefore, at high frequency, Co^{2+} ions have a stronger affinity for oxygen than Ni^{2+} ions, so the increasing cobalt substitution can inhibit the appearance of Fe^{2+} ions which results in the ε' decreases.

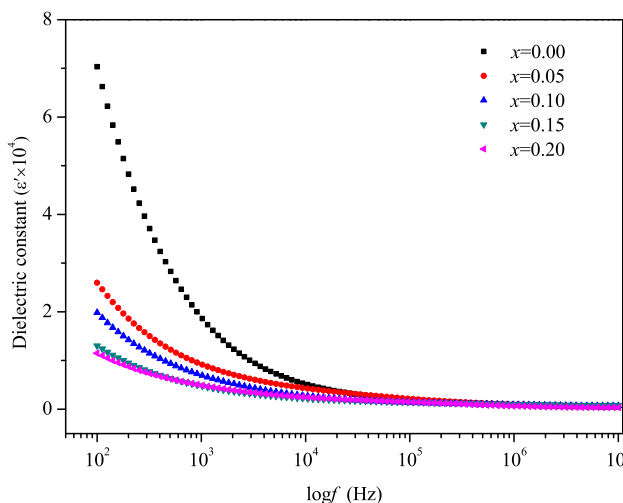Figure 6a shows the dc resistivity (ρ) temperature spectrum of NZCF ferrites, which well reflects the
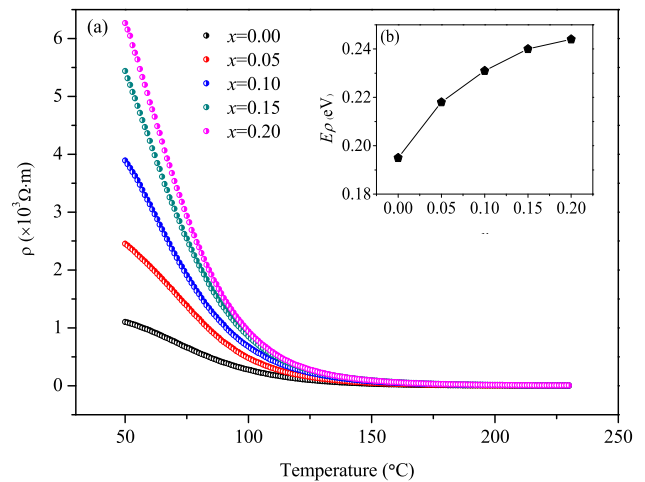
Fig. 6 Resistivity ρ temperature spectrum (**a**) and E_ρ with x (**b**) of NZCF ferrites

exponential decline with temperature rise and shows the classic semiconductor behavior. Also, ρ monotonously increases with the addition of Co substitution and achieves the maximum value (6.27 × 10³ Ω•m) at $x = 0.20$. The change of resistivity is due to the conduction mechanism of electronic migration ($Fe^{2+} \leftrightarrow Fe^{3+} + e^-$) in ferrite. As discussed earlier, the more Co^{2+} ions substituted, the less Fe^{2+} ions, which weakens the electronic migration, and thus increases the ρ.

The electron hopping ability is also closely related to activation energy [28]. Activation energy (E_ρ) can be calculated by equation $\rho = \rho_0 \exp(E_\rho/kT)$ [29]. Figure 6b reveals that E_ρ increases from 0.195 to 0.244 eV with x from 0 to 0.2, confirming that Co substitution affects E_ρ. According to the above discussion, the replacement of Ni^{2+} ion by Co^{2+} ions reduces the amount of Fe^{2+} ions, making it difficult for its local electrons to overcome barriers and obstacles. Therefore, E_ρ gradually increases with the addition of cobalt substitutions.

4 Conclusion

We have been systematically studied Co-substituted NiZn ferrite ($Ni_{0.7-x}Zn_{0.3}Co_xFe_2O_4$, $0 \leq x \leq 0.20$) with the crystal structure and magneto-electric performances for different cobalt substitutions. The Lattice parameter (a) and average grain size (D) increase with cobalt addition. The initial permeability (μ_i) achieves a maximum value (123, $x = 0.05$). The

Fig. 5 Frequency spectrum of dielectric constant ε' of NZCF ferrites

highest saturation magnetization (Ms) is 83.14 emu/g ($x = 0.15$), and the lowest coercivity (Hc) is 13.25 Oe ($x = 0.05$). Meanwhile, the dielectric spectrum shows that real dielectric constant (ε') exhibits the classical relaxation frequency characteristics: it exhibits a large ε' at low frequency, and when the frequency increases, ε' drops sharply near relaxation, and finally remains stable. Since the reduction of Fe^{2+} ions, the dc resistivity (ρ) and the activation energy (E_ρ) increase with Co substitution. Based on the above research, the sample with $x = 0.05$ Co-substituted NiZn ferrite possesses optimum comprehensive performance with high initial permeability (μ_i, 123@10 kHz), relative high saturation magnetization (Ms, 78.25 emu/g) and low coercivity (Hc, 13.25Oe). These findings are expected to be applied to electronic components such as inductors, transformers and filters.

Acknowledgements

References

1. H. Fujimori, H. Yoshimoto, T. Masumoto, T. Mitera, Anomalous eddy current loss and amorphous magnetic materials with low core loss. J. Appl. Phys. **52**, 1893 (1981)

2. Q. Chen, P. Du, W. Huang, L. Jin, W. Weng, G. Han, Ferrite with extraordinary electric and dielectric properties prepared from self-combustion technique. Appl. Phys. Lett. **90**, 132907 (2007)

3. A.V. Humbe, J.S. Kounsalye, M.V. Shisode, K.M. Jadhav, Rietveld refinement, morphology and superparamagnetism of nanocrystalline $Ni_{0.70-x}Cu_xZn_{0.30}Fe_2O_4$ spinel ferrite. Ceram. Int. **44**, 5466–5472 (2017)

4. Z. Yan, J. Luo, Effects of Ce–Zn co-substitution on structure, magnetic and microwave absorption properties of nickel ferrite nanoparticles. J. Alloys Compd. **695**, 1185–1195 (2017)

5. S.A. Saafan, T.M. Meaz, E.H. El-Ghazzawy, M.K. El-Nimr, M.M. Ayad, M. Bakr, AC and DC conductivity of NiZn ferrite nanoparticles in wet and dry conditions. J. Magn. Magn. Mater. **322**, 2369–2374 (2010)

6. L.Z. Li, X.X. Zhong, R. Wang, X.Q. Tu, L. He, R.D. Guo, Z.Z. Yu, Structural, magnetic and electrical properties in Al-substituted NiZnCo ferrite prepared via the sol-gel auto-combustion method for LTCC technology. RSC Adv. **7**, 39198–39203 (2017)

7. L.Z. Li, X.X. Zhong, R. Wang, X.Q. Tu, L. He, F.H. Wang, Effects of Ce substitution on the structural and electromagnetic properties of NiZn ferrite. J. Magn. Magn. Mater. **475**, 1–4 (2019)

8. P. Yang, Z.Q. Liu, H.B. Qi, Z.J. Peng, X.L. Fu, High-performance inductive couplers based on novel Ce^{3+} and Co^{2+} ions co-doped NiZn ferrites. Ceram. Int. **45**, 13685–13691 (2019)

9. B.P. Rao, O.F. Caltun, Microstructure and magnetic behavior of Ni–Zn–Co ferrites. J. Adv. Mater. **8**, 995–997 (2006)

10. P.G. Bercoff, H.R. Bertorello, Localized canting effect in Zn substituted Ni ferrites. J. Magn. Magn. Mater. **213**, 56–62 (2000)

11. E. Rezlescu, L. Sachelarie, P.D. Sachelarie, N. Rezlescu, Effect of substitution of divalent ions on the electrical and magnetic properties of Ni–Zn–Me ferrites. IEEE. Trans. Magn. **36**, 3962–3967 (2000)

12. L.Z. Li, X.X. Zhong, R. Wang, X.Q. Tu, L. Peng, Structural and magnetic properties of Co-substituted NiCu ferrite nanopowders. J. Magn. Magn. Mater. **433**, 98–103 (2017)

13. D.F. Wan, X.L. Ma, *The Physics of Magnetism* (UESTC Press, Chengdu, 1994)

14. R. Kumar, H. Kumar, R.R. Singh, P.B. Barman, Variation in magnetic and structural properties of Co-doped Ni-Zn ferrite nanoparticles: a different aspect. J. Sol-Gel Sci. Technol. **78**, 566–575 (2016)

15. X.H. Wu, L.Z. Li, X.X. Zhong, R. Wang, X.Q. Tu, L. He, F.H. Wang, Effects of HfO_2 dopant on the structure, magnetic and electrical properties of NiZnCo ferrites. Ceram. Int. **45**, 10776–10781 (2019)

16. M. Drofenik, A. Znidarsic, D. Makovec, Influence of the addition of Bi_2O_3 on the grain growth and magnetic permeability of MnZn ferrites. J. Am. Ceram. Soc. **81**, 2841–2848 (1998)

17. Y.J. Huang, W.S. Li, Z.W. Lan, *Magnetic Materials* (UESTC Press, Chengdu, 1993)

18. F. Xu, H. Zhang, F. Xie, Y. Liao, Y. Li, J. Li, L. Jin, Y. Yang, G. Gan, G. Wang, Investigation of grain boundary diffusion and grain growth of Lithium Zinc Ferrites with low activation energy. J. Am. Ceram. Soc. **101**, 5037–5045 (2018)

19. P.J. Zagg, P.J. Valk, M.T. Rekveldt, A domain size effect in the magnetic hysteresis of NiZn-ferrites. Appl. Phys. Lett. **69**, 2927–2929 (1996)

20. Z.Q. Liu, Z.G. Peng, C.C. Lv, X.L. Fu, Doping effect of Sm^{3+} on magnetic and dielectric properties of Ni-Zn ferrites. Ceram. Int. **43**, 1449–1454 (2017)

21. K. Jalaiah, K.V. Babu, K.C. Mouli, P.S.V. Subba Rao, Effect on the structural, DC resistivity and magnetic properties of Zr and Cu co-Substituted $Ni_{0.5}Zn_{0.5}Fe_2O_4$ using sol-gel auto-combustion method. Phys. B **534**, 125–133 (2018)

22. M. Kaiser, Effect of rare earth elements on the structural, magnetic and electrical behavior of Ni-Zn-Cr nanoferrites. J. Alloys Compd. **719**, 446–454 (2017)

23. P. Thakur, R. Sharma, M. Kumar, S.C. Katyal, P.B. Barman, V. Sharma, P. Sharma, Structural, morphological, magnetic and optical study of co-precipitated Nd^{3+} doped Mn-Zn ferrite nanoparticles. J. Magn. Magn. Mater. **479**, 317–325 (2019)

24. M.A. Almessiere, Y. Slimani, S. Güner, M. Nawaz, A. Baykal, F. Aldakheel, S. Akhtar, I. Ercan, İ. Belenli, B. Ozçelik, Magnetic and structural characterization of Nb^{3+}-substituted $CoFe_2O_4$ nanoparticles. Ceram. Int. **45**, 8222–8232 (2019)

25. W.W. Wang, C.W. Wang, J.J. Zheng, F.L. Shang, J.S. Dang, X. Zhao, Directional Diels-Alder cycloaddions of isoelectronic graphene and hexagonal boron nitride in oriented external electric fields: reaction axis rule vs polarization axis rule. Nanoscale **12**, 15364–15370 (2020)

26. B. Marfoua, J. Hong, Electric filed dependent valley polarization in 2D $WSe_2/CrGeTe_3$ heterostructure. Nanotechnology **31**, 425702–425718 (2020)

27. K.W. Lee, C.E. Lee, Strain-induced topological phase transition with inversion of the in-plane electric polarization in tiny-gap semiconductor SiGe monolayer. Sci. Rep. **10**, 11300–11310 (2020)

28. A. Lakshman, P.S.V.S. Rao, B.P. Rao, K.H. Rao, Electrical properties of In^{3+} and Cr^{3+} substituted magnesium–manganese ferrites. J. Phys. D **38**, 673–678 (2005)

29. U.V. Chhaya, R.G. Kulkarni, Metal-insulator type transition in aluminium and chromium co-substituted nickel ferrites. Mater. Lett. **39**, 91–96 (1999)